

P8 Exploring new Architectures for Compressed Sensing Reconstructions in the MeerKAT era

Jonas Schwammberger

January 23, 2019

Abstract

MeerKAT new Radio Interferometer, poses a large scale image reconstruction problem.

Compressed sensing reconstructions for Radio astronomy exist, but are slower than CLEAN.

Compressed Sensing and CLEAN use the same architecture, both use Major Cycle. In this work, we explore if Compressed Sensing reconstructions can be made faster with in a different architecture

Several possibilites are discussed and a new proof-of-concept algorithm is developed, which does not require a Major Cycle. We estimate the minimum runtime complexity of the algorithm and compare it to CLEAN.

However, the algorithm is not suitable in the context of meerkat reconstructions. It requires too much memory and

we come to the conclusion that in the context of MeerKAT reconstructions, the Major Cycle architecture is easier to compute.

No obvious contender to replace the Major Cycle.

Contents

1 Compressed Sensing Image Reconstruction for MeerKAT	1
1.1 The basic Measurement Equation of a radio interferometry	1
1.2 The Major Cycle Architecture	2
2 Challenges for imaging MeerKAT data	4
2.1 Wide Field of View Imaging and the third Fourier Component	4
2.1.1 State of the art: w -stacking algorithm	5
2.2 Self-Calibration	6
3 Eliminating the Major Cycle	7
3.1 Separating the Major Cycle into two Optimization Problems	7
3.2 Reconstruction on the Sphere	8
3.3 Direct Fourier Transform	8
4 Compressed Sensing with direct Fourier Transform and Coordinate Descent	10
4.1 The Starlet Transform	11
4.1.1 Handling the positivity constraint	13
4.2 Coordinate Descent Implementation	13
4.3 Iteration scheme	13
4.3.1 Non-uniform FFT approximations	14
5 Test on Simulated Data	15
5.1 Super-resolution of two point sources	15
5.2 Super resolution of mixed sources	16
6 Runtime cost comparison on a real-world MeerKAT reconstruction	18
6.1 Cost function of an idealized Coordinate Descent	18
6.2 Cost function of WSCLEAN	19
6.3 Comparison on a MeerKAT reconstruction problem	19
6.4 Embracing the Major Cycle	21
7 Compressed Sensing reconstructions in the MeerKAT era	22
8 Ehrlichkeitserklärung	26

1 Compressed Sensing Image Reconstruction for MeerKAT

An instrument in the real world measures noisy data. Measurements are corrupted by noise, interference sources or the measurement instrument itself. Image reconstruction problems appear when one tries to remove the corruption from the measurements and tries to find the observed image of the instrument. This leads to an ill-posed inverse problem: A small change in the measurements may create very different image reconstructions, and many possible images match the measurements. An image reconstruction algorithm therefore has to find the observed image from a potentially large set of possible images.

In the past, image reconstructions applied simple heuristics and approximated a likely image. How close the approximation was to the observed image was in general not known. The theory of compressed sensing[1][2] introduced a new theoretical framework under which image reconstructions can be analysed. This has lead rise to new compressed sensing reconstruction algorithms, which under the right conditions are guaranteed to reconstruct the observed image. Furthermore they have shown super-resolution performance in real-world environments, creating reconstructions above the accuracy limit of the instrument.

This work applies compressed sensing image reconstruction to the field of radio astronomy. The new MeerKAT radio interferometer poses a reconstruction problem on a new scale of data volume. The raw measurements easily take up several terabytes of disk space. The focus of this work is creating a scalable compressed sensing image reconstruction algorithm.

The current state of the art reconstruction algorithm for MeerKAT is based on CLEAN[3][4]. It is a reconstruction using a simple heuristic and was developed before the theory of compressed sensing was known. In recent years, compressed sensing reconstruction algorithms were developed for radio interferometers[5][6][7]. They beat CLEAN in terms of reconstruction quality, producing super-resolved reconstructions. However, CLEAN has the upper hand in runtime complexity. Therefore, an efficient implementation of CLEAN is still the go to reconstruction algorithm for MeerKAT data.

The efficient implementation use CLEAN in the Major Cycle Architecture, which was developed with CLEAN in mind. Current compressed sensing algorithms use a similar architecture. So far, little research has gone into different architectures for compressed sensing reconstructions in radio astronomy. This work explores different architectures for compressed sensing reconstructions with the hope of reducing the computational complexity.

A new proof-of-concept reconstruction algorithm was developed with a simplified architecture. It was tested on simulated MeerKAT data and the lower-bound asymptotic complexity was evaluated. The new algorithm scales independently of the image size, but scales worse with the number of input measurements compared to CLEAN. For the MeerKAT image reconstruction, the number of input measurements tends to be the largest of all numbers in the problem. Even though the algorithm could be improved further, it is unlikely to beat CLEAN reconstructions in terms of runtime complexity on MeerKAT data.

1.1 The basic Measurement Equation of a radio interferometry

Real world radio interferometers have complicated measurement equations. They become even more complicated for large interferometers like MeerKAT. These problems get addressed in section 2. This section looks at the basic measurement equation of a radio interferometer (1.1) and discusses the two fundamental challenges for radio interferometry image reconstruction.

$$V(u, v) = \int \int I(x, y) e^{2\pi i(ux+vy)} dx dy \quad (1.1)$$

An interferometer measures Fourier Components V (called Visibilities in Radio Astronomy) from the sky image I at position x and y . The term $e^{2\pi i(ux+vy)}$ represents the two dimensional Fourier Transform. The task is to reconstruct the observed image I from the measured Visibilities V . In theory this task is trivial: Since the inverse Fourier Transform exists, we can reconstruct the image I by calculating the inverse Fourier Transform of V . However, two properties of the Visibilities make this task challenging in practice:

1. Non-uniform sampling pattern in Visibility space
2. Incomplete Visibility coverage.

Property 1: We want to reconstruct an image with uniformly spaced pixels. The instrument defines the sampling pattern in Visibility space and does not correspond to the exact pixels of the reconstructed image. This property keeps us from using the Fast Fourier Transform. The naive inverse Fourier Transform can still be calculated, but it has a quadratic runtime and does not scale to the data volume of interferometers. Current reconstruction algorithms use the non-uniform Fast Fourier Transform. The non-uniform FFT approximates the non-uniform Fourier Transform.

Property 2: Interferometers sample only a limited set of Visibilities. It does not have all information for reconstruction. When the inverse Fourier Transform is applied on the Visibilities, the resulting image is corrupted by the incomplete Visibilities. It contains structures which were introduced by the interferometer and were not observed. With only knowing the incomplete set of Visibilities a reconstruction algorithm has to decide which image structures were truly measured, and which are due to the instrument. This forms an ill-posed inverse problem. There are many images that fit the measurements, and a small change in the Visibilities can lead to a very different reconstruction.

CLEAN represents the instrumental effect with a Point Spread Function (PSF). After the non-uniform FFT produced the 'dirty' image, CLEAN tries to reconstruct observed image with a deconvolving the 'dirty' image with the PSF. Note however that both CLEAN nor the non-uniform FFT are approximations. In real world reconstructions, these two approximations are used in the major cycle architecture to increase the reconstruction accuracy.

1.2 The Major Cycle Architecture

Major cycle was created with CLEAN in mind. Compressed sensing reconstructions use essentially the same architecture with minor modifications.

A CLEAN image reconstruction for radio interferometers consists of two different steps: A non-uniform FFT, which approximates the inverse Fourier Transform efficiently and an deconvolution algorithm, which approximates the instrumental effects on the image (typically based on CLEAN). These two approximations are an error source of the reconstruction. The major cycle architecture 1 therefore tries to iteratively minimize the errors of the non-uniform FFT and the deconvolution over several iterations.

The first major cycle uses the non-uniform inverse FFT to approximate the 'dirty' image from the Visibilities. The deconvolution algorithm decides parts which belong to the observed image and which are due to instrumental and other noise effects. It returns the noise part of the image, which gets transformed back into residual Visibilities. The next major cycle iteration continues with the

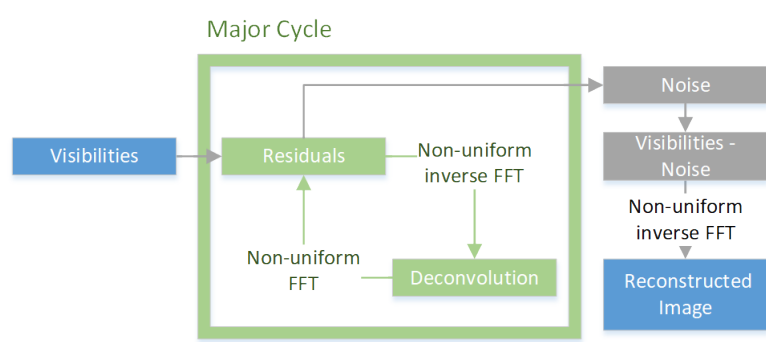


Figure 1: The Major Cycle Framework

residual Visibilities. The residual Visibilities get minimized until they contain only the instrumental effects and noise.

After several major cycles the residual on a regularly spaced image which has a small error from non-uniform samples, and a small error from incomplete measurements.

Compressed sensing reconstructions essentially use the same architecture, although with minor alterations. In general, they keep a similar scheme of forward/backward non-uniform FFT, but do not use a deconvolution in image pace. Instead, they analyse constraints defined on the image (For example all pixels should be non-negative), and try to find the Visibilities that minimize the constraint violations.

For CLEAN reconstructions, the forward/backward non-uniform FFT are the most expensive operations, while the deconvolution is negligible. The compressed sensing algorithms tend to require more major cycle iterations to converge and the image constraint analysis tends to be more expensive than CLEAN deconvolutions. Current research into compressed sensing reconstructions is focussed on reducing the number of major cycles[6].

2 Challenges for imaging MeerKAT data

New interferometers like MeerKAT put additional challenges on the image reconstruction problem. First, the new instrument produce a new magnitude of data, forcing reconstruction algorithms to be highly scalable and distributable. Second, the more sensitive instruments with large field of view amplify effects which were negligible in older instruments, like non-coplanar baselines or the ionosphere.

Compressed sensing has to be able to work with these issues somehow. Solutions all in the context of the major cycle, a new architecture may need to handle effects differently. Hopefully in a manner that is at least as efficient.

In this work, the effects of non-coplanar baselines gets handled in more detail. The effect has a neat mathematical notation, it adds a third fourier component to the measurement equation, but breaks the two dimensional fourier relationship introduced in section 1.1.

Calibration used to be a task before image reconstruction. Calibration gets not explicitly handled here, but it is important to keep in mind. For older interferometers, the data was calibrated before image reconstruction. With the advent of self-calibration, the image reconstruction is also used to improve calibration. MeerKAT requires more calibration parameters, so an image reconstruction algorithm has to be able to calibrate, or it is not interesting.

Further issues that do not get handled here

- (Beam Pattern, A Projection)
- Full polarization
- Wide band imaging

There are several challenger for imaging meerkat data. One problem is the new amount of data.

terabytes of measurements. Large image size 32k squared are the obvious problems to solve. Distributing the problem is not part of this work.

In this work, it is focused on Wide field of view issue.

2.1 Wide Field of View Imaging and the third Fourier Component

The measurement equation of radio interferometers contains a third fourier component, the w component. This leads to the following wide field of view measurement equation (2.1).

$$V(u, v, w) = \int \int \frac{I(x, y)}{\sqrt{1 - x^2 - y^2}} e^{2\pi i [ux + vy + w(\sqrt{1 - x^2 - y^2} - 1)]} dx dy \quad (2.1)$$

For small field of view observations, the term $\sqrt{1 - x^2 - y^2} \approx 1$, and we arrive at the basic measurement equation (1.1). For small field of view, the w term can be ignored, and the image can be calculated with the inverse two dimensional non-uniform FFT. For wide field of view measurements, the w term breaks the two dimensional Fourier relationship. The measurement equation (2.1) can still be inverted, but the resulting algorithm has a quadratic runtime and is not feasible in practice.

Note that the image $I(x, y)$ of the wide field of view the measurement equation (2.1) is still two dimensional, even though the Visibilities $V(u, v, w)$ have three. The relationship between Visibilities and image is neither the two, nor the three dimensional Fourier transform. The Visibilities represents an image on the celestial

sphere. This means the image is naturally curved, and the w component represents the distortion introduced by the curvature.

One can simply ignore the w component, ignore the curvature and use the two dimensional Fourier Transform. The image then does not lie on a sphere, but on a tangent plane. At the tangent point (where $\sqrt{1 - x^2 - y^2} \approx 1$, typically the image center in radio astronomy) the two reconstructions are identical. But the distortion gets more severe away from the tangent point. The image 2a shows a tangent plane reconstruction over a large field of view, while 2b shows the same reconstruction but w corrected. Close to the tangent point, the image center, the reconstructions both locate the point sources. At the image edges, the distortion gets severe enough to decorrelate the Visibilities and the point sources get 'torn' apart.

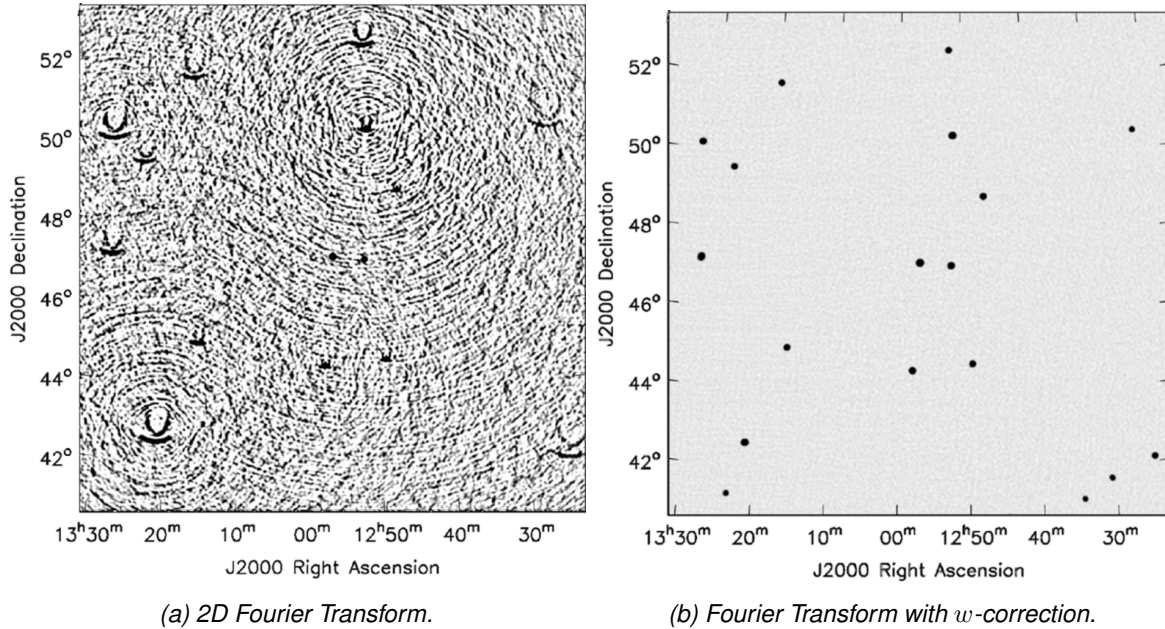


Figure 2: Celestial sphere distortion on simulated data. Source: [8]

Image reconstructions for MeerKAT need to account for the w component efficiently. In the Major Cycle framework, this is part of the non-uniform FFT. The first approach was to image facets, creating several tangent planes for the celestial sphere. A more efficient approach came in the form of the w -projection algorithm[8]. It uses convolution on the Visibilities during the non-uniform FFT. MeerKAT currently uses the w -stacking algorithm, which is more efficient than w -projection on MeerKAT's data volume and is simple to distribute.

This is still an active field of research. The latest work as of time of writing is a hybrid approach[9] with both w -stacking and w -projection. As of time of writing, it was not yet adapted.

2.1.1 State of the art: w -stacking algorithm

Here a short explanation of the w -stacking algorithm is provided. It is a surprisingly simple algorithm that seems to be here to stay. It is a modification of the nuFFT operation displayed in figure 1.

Inverse nuFFT with w -stacking: Visibilities get grouped into stacks by their w -term. Every visibility inside a stack has a similar w -term. The more stacks, the more accurately you can handle the w component. The figure displays the relation

The nuFFT gets called on each stack separately, and a constant w correction factor applied. Since w -term is constant, we can use the two dimensional nuFFT again. At the end, all the stacks are summed together to form the dirty image.

nuFFT with w-stacking: The inverse is done in a similar fashion. The sum cannot be re-separated, so the image gets copied into each stack. The constant w factor gets divided out. The nuFFT gets applied.

the runtime

(talking about more recent hybrid approach, limiting the total number of ?w-stacks?)

2.2 Self-Calibration

Complex gain term. Corrects amplitude and phase.

Traditional Calibration

A calibration source close by, with a known brightness. Phase and amplitude calibration was done before image reconstruction. For older interferometers, there was a very limited number of calibration terms to solve.

but again effects of wide field of view also increase the number of necessary calibration terms. The advent of self calibration, in which the image reconstruction was used to solve for both, the observed image and the calibration of the instrument.

Self calibration with the major cycle algorithm and a CLEAN deconvolution.

Initial phase calibration Shallow clean phase calibration deep clean phase and amplitude calibration deep clean reconstruction

3 Eliminating the Major Cycle

There is little research in exploring a different architecture for Compressed Sensing. The closest to this work was done by Pratley et al[10], which optimizes the non-uniform FFT in the context of compressed sensing. The Major cycle is still used. On the upside, progress in w-term accuracy and runtime.

There are ways to form a different architecture. However, the advent of self-calibration pushes a forward-backward kind of architecture on the reconstruction.

3.1 Separating the Major Cycle into two Optimization Problems

The major cycle reduces two errors simultaneously. The error introduced by the non-uniform FFT approximation, and the error introduced by the deconvolution approximation. In a sense, the major cycle is a simple optimization algorithm: It iteratively calls the non-uniform FFT and deconvolution approximations with the error from the last iteration, until the error is below a certain threshold.

$$FT : \underset{I_{dirty}}{\text{minimize}} \|V - A^{-1}I_{dirty}\|_2^2 \quad (3.1)$$

$$\text{deconvolution} : \underset{x}{\text{minimize}} \|I_{dirty} - x \star PSF\|_2^2 + \lambda \|P(x)\|_1 \quad (3.2)$$

The major cycle can also be separated into two objectives (3.1) and (3.2), and solved in sequence. The first objective (3.1) tries to find the best uniformly spaced image I_{dirty} matching the observation. A^{-1} represents the non-uniform inverse FFT approximation ($A^{-1}I_{dirty} \approx F^{-1}I_{dirty}$). When this is solved, the original Visibility measurements are not needed any more. Then, the second objective (3.2) searches for the deconvolved image x regularized by some prior $P()$.

By separating the two objectives, the hope is we can use specialized optimization algorithms that overall converge faster than several major cycles. Also, after the first objective was minimized, we can drop the Visibilities, which can be magnitudes larger than the image.

At first glance, this is a sensible idea, but the devil is in the objective (3.2). Namely in the PSF is not constant, it varies over the image. In the Major Cycle Architecture, a constant PSF^1 is sufficient: It only needs to approximate the deconvolution. The error introduced by a constant PSF can be reduced in the next Major Cycle. By eliminating the Major Cycle, we also eliminated the chance to approximate the deconvolution with a constant PSF . In the worst case, we would need to estimate the PSF for each pixel in the image.

In the worst case, these many PSF s may stop us from using this approach. It is plausible that can use fewer PSF s and be close enough. No known work done in the radio astronomy. The Major Cycle is ubiquitous. But it is plausible.

However, the problem is that the imaging algorithm should also be able to calibrate. With this approach, there is a strict one way flow from measurements to image. For calibration, a backwards flow from image to measurements is necessary.

For calibrated data, this approach may be potentially faster. but since MeerKAT will be difficult to calibrate correctly, this is unlikely.

Fourier Transform for PSF

¹CLEAN implementations in Radio Astronomy typically use a constant PSF . This is not strictly necessary, one can also implement CLEAN with a varying PSF .

3.2 Reconstruction on the Sphere

The signal naturally lives on the celestial sphere.

Not that much used in Radio Astronomy reconstructions. Work that uses to project on the sphere and looks at the reconstruction quality [11].

The wide field of view measurement equation (2.1) can be expanded into spherical harmonics.

[12] measurement equation with spherical harmonics. Essentially replaces the non-uniform FFT from the Major cycle with a new approach based on the fact that it has a solution to the Helmholtz equation. , see [12] for further detail. It can be used as a different way to arrive at a dirty image from wide field of view interferometers. It is useful in full sky image, because it fulfills the (property from paper) and the full sky dirty image does not have artifacts. It does not gain any complexity advantage, quite the contrary.

Even if the spherical harmonics transform would gain a speed advantage, used in the way of [12] it would still be the same major cycle architecture, just with spherical harmonics transform.

However there is the possibility to just do everything on the sphere.

Spherical haar wavelets used for simulating visibilities from a known image, essentially the opposite operation from imaging. [13]

based on the spherical harmonic transform. Doing a Spherical harmonic transform efficiently is still an active field of research [14]

transform . The wide field of view measurement equation (2.1) can be factorized into spherical harmonics. This means spherical harmonics are equivalent, calculating an image from the measurements with the three dimensional fourier transform is the same as using the spherical harmonics transform. [15]

[16]sampling theorem on a sphere

Spherical harmonics were researched in the context of Compressed Sensing image reconstructions (cite wiaux). They improved the quality of the image reconstruction, but no speed advantage.

The push on solving on the sphere directly. Using spherical haar wavelets, (cite) was able to speed up the simulation problem. Simulation tries to solve to problem of finding the measurements corresponding to a given image x . However, this has so far not been used for imaging.

3.3 Direct Fourier Transform

Hardy et al[17] handled the whole inverse Fourier Transform as an explicit matrix F^{-1} of size $M * N$. They dropped the non-uniform FFT and w -stacking approximations. This is trivially to distribute later. The only problem is of Course that for MeerKAT data sizes $M * N$ is too large (4gb of visibilities times 1 Billion Pixels).

However there is potential for improvement: Only a limited number of pixels in a reconstruction are not zero. We spent a lot of processing power on pixels which do not matter in the reconstruction. If we could predict which pixels are not zero, we would only need to calculate a subset of F^{-1} columns to reconstruct the image. The starlet transform[18] has a way to predict its non-zero components. We represent the image as a combination of starlets, and estimate which starlets are likely non-zero from the Visibilities directly.

To my knowledge, such an algorithm has never been tried out.

A proof-of-concept algorithm was developed that shows the prediction actually works in practice. It uses Coordinate Descent with the starlet transform, and only needs to calculate a subset of the matrix F^{-1} for a

reconstruction. The question remains how many columns of F^{-1} are needed, and is it more efficient than an algorithm using the major cycle architecture.

4 Compressed Sensing with direct Fourier Transform and Coordinate Descent

Instead of using the Major Cycle architecture and approximate the non-uniform FFT approximation, we directly use the Fourier transform matrix F . We show the principle of our approach and of Compressed Sensing reconstructions in general at a simplified example. Let us minimize the objective function (4.1).

$$\underset{x}{\text{minimize}} \quad \|V - Fx\|_2^2 + \lambda \|x\|_1 \quad (4.1)$$

The data term $\|V - F^{-1}x\|_2^2$ forces our image to be similar to the measurements, and the regularization term $\|x\|_1$ tells us how likely the current reconstruction is to be the true image. With our term we assume our image contains only a limited number of non-zero pixels, or that it only contains a few stars, which fill only a single pixel. The parameter λ weights the trade-off between the data and the regularization term.

Note in the one dimensional case, where we only have one pixel, the data term of the objective (4.1) forms a parabola and the regularization term a shrink operation². The optimum for a single pixel can be calculated by solving for the minimum of the parabola first, followed by a shrink operation. With Coordinate Descent we can exploit this property. We fix all pixels except for one and iteratively find the current minimum of each pixel. Now when we continually iterate over all pixels several times, we eventually converge to a solution. The full Coordinate Descent algorithm can be implemented in a few lines of python code:

```

1 def coordinate_descent(V_residual, x, lambda, max_iter):
2     for k in range(0, max_iter):
3         for i in pixels_row:
4             for j in pixels_column:
5                 x_old = x[i, j]
6                 fourier_column = calculate_fourier_transform(i, j)
7                 fr = real(fourier_column)
8                 fi = imag(fourier_column)
9                 rr = real(V_residual)
10                ri = imag(V_residual)
11
12                #find apex
13                a = sum(fr**2 + 2*fr*fi + fi**2)
14                b = sum(fr*rr + fr*ri + fi*rr + fi*ri)
15                x_new = b / a + x_old
16
17                x_new = shrink(x_new, lambda)
18                x[i, j] = x_new
19                V_residual = V_residual - fourier_column * (x_new - x_old)

```

Coordinate Descent has to iterate over every pixels possibly several times. How quickly Coordinate Descent converges in theory is not well understood. Optimizing our function (4.1) falls in the class of quadratic programming, with a strictly convex objective. In this case, Coordinate Descent is guaranteed to converge at least linearly[19]. Sadly, real-world objective functions for image reconstruction are often not strictly convex. Usually our image is constrained to have only positive pixels[11], which breaks the strictly convex property of our objective. In our environment, the convergence guarantees of Coordinate Descent are not well understood in theory.

²The shrink operation reduces the magnitude of the pixel by λ . For example: Pixel $x = -12.4$, $\lambda = 0.6$. The new pixel value after shrinkage follows as $\text{shrink}(-12.4, 0.6) = -11.9$

In practice, Coordinate Descent can be improved with heuristics. Since we assume our image contains only a few stars, a few non-zero pixels, the simple Coordinate Descent algorithm wastes resources checking if the pixel is still zero. A better scheme would be the active set heuristic[20]: We iterate over every pixel once. Then, for a given number of iterations, we only check the pixels that have changed. This is an improvement, but impossible in the context of MeerKAT. We have too many pixels and Visibilities, iterating over every pixel once is too expensive.

However, it turns out we do not need to if we imitate CLEAN: For CLEAN, the non-uniform FFT approximates the 'dirty' image, which is corrupted by the effects of incomplete measurements. CLEAN then subtracts a fraction of the PSF at the largest pixel value. In other words, the largest pixel value in the dirty image is the most likely non-zero pixel. We can use the dirty image approximation for a 'probability distribution' of non-zero pixels. It does not need to be accurate, since the actual reconstruction is done with the direct Fourier Transform.

This is, in principle, how the proof-of-concept algorithm works. Instead of reconstructing an image, it reconstructs in the starlet space. It uses the starlet transform of the dirty image to find likely non-zero components. Coordinate Descent is used to optimize single starlets. A proof-of-concept version of this algorithm was developed in python.

Although the algorithm produces super-resolved images in section 5, it is currently not known if it actually converges to the true optimum. Finding all relevant non-zero starlets is left to the heuristic, there may be conditions under which it never includes relevant components. Further convergence analysis was outside the scope of the project. Also note that for this implementation, every time likely non-zero components are searched, it simply uses the non-uniform FFT for the dirty image approximation. This was done for simplicity's sake and can be improved.

4.1 The Starlet Transform

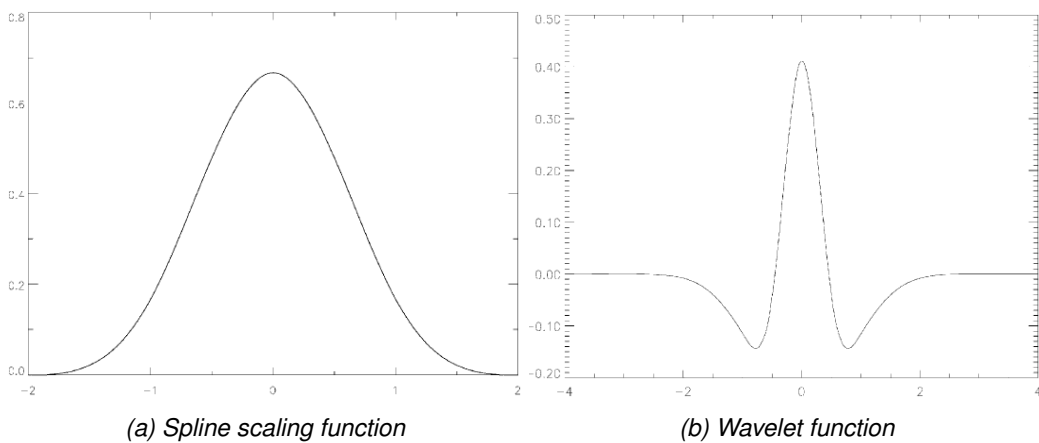


Figure 3: Scaling and wavelet function of the starlet wavelet. Source: [18]

The starlet transform is an Isotropic Undecimated Wavelet Transform (IUWT) with the starlet wavelet shown in figure 3. As such, it defines two operations: The transformation from starlet into image space which is called synthesis, and the inverse which is called decomposition. The starlet space represents an image in multiple layers at different scales, where lower layers contain smaller objects and upper layers the extended emissions. The lowest starlet layer represents the stars, while the upper layer represents the largest hydrogen clouds in

the image.

$$\begin{aligned} c_0 &= \mathbf{x} \star B_0 \\ \mathbf{w}_0 &= \mathbf{x} - c_0 \end{aligned} \tag{4.2}$$

Let us look at the lowest starlet layer first, and how it is calculated from the image. B , and \mathbf{x} . $\mathbf{x} - c_0$ removes the larger structures from the image, leaving us with the smallest in w_0 . Does are not the starlet components, α_0 . However, we can estimate them with a shrink operation. we can then convolve α with the starlet function to get back to w_0 . In our implementation

In this case, we use it for estimating likely non-zero α . Figure 4 shows an example for the lowest starlet layer.

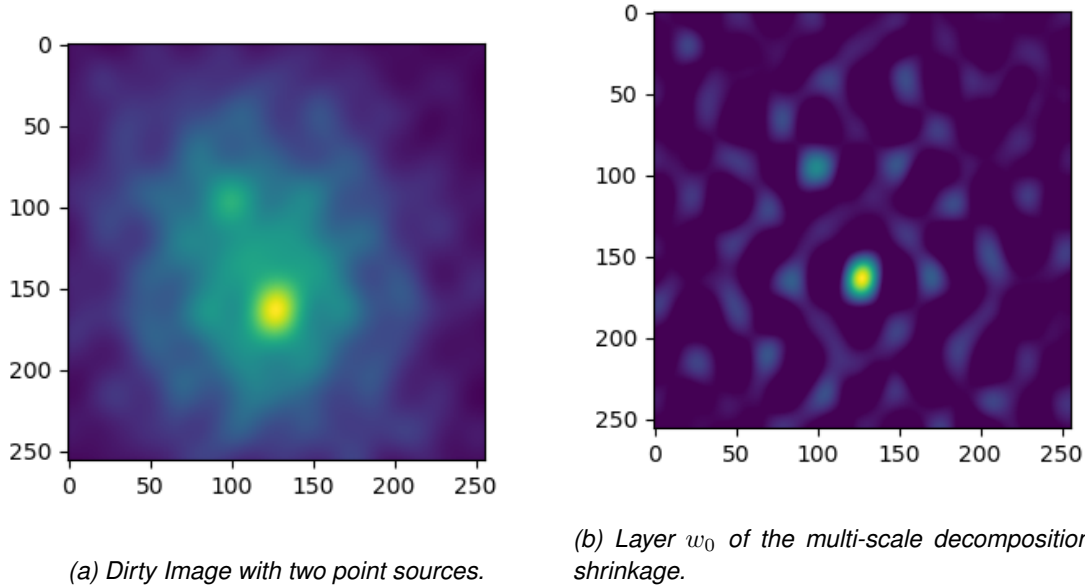


Figure 4: Dirty map and w_0 starlet layer. The right image shows the probability distribution for point sources in the dirty image.

The full decomposition is then just repeated for each intermediate layer w_i . (4.3) !!!!!A trous algorithm, size of the different S_i . The last, heavily blurred c_J contains the structures which were too big to represent with the largest starlets, and is the last layer of the decomposition.

$$\begin{aligned} c_0 &= \mathbf{x} \star B_0 & c_1 &= c_0 \star B_1 & \dots & c_{J-1} &= c_{J-2} \star B_{J-1} & \mathbf{c}_J &= c_{J-1} \star B_J \\ \mathbf{w}_0 &= \mathbf{x} - c_0 & \mathbf{w}_1 &= c_0 - c_1 & \dots & \mathbf{w}_{J-1} &= c_{J-2} - c_{J-1} \end{aligned} \tag{4.3}$$

The synthesis transform however is easy.

$$\mathbf{x} = \mathbf{w}_0 + \mathbf{w}_1 + \dots + \mathbf{w}_{J-1} + \mathbf{c}_J \tag{4.4}$$

The starlet decomposition is over-complete.

The difference between α and w_i is not always important. For the SASIR algorithm, for FISTA, which is how [5] used the starlet transform for regularization, shrinkage on w_i without convolution.

For FISTA, this is irrelevant, but for Coordinate descent it is important. note on the shrinkage the original starlet people [18] does not differentiate between α and w_i , and neither did [5]. For the Coordinate Descent implementation it is relevant for handling the positivity constraint.

4.1.1 Handling the positivity constraint

As mentioned in section 4, image reconstruction algorithms for radio astronomy typically constrain the image to be non-negative[11].

4.2 Coordinate Descent Implementation

We have the starlet regularization, let us put it into an algorithm. Start with the

$$\underset{\alpha}{\text{minimize}} \ \|V - FD\alpha\|_2^2 + \lambda \|\alpha\|_1 \quad (4.5)$$

Proof of concept implementation. There are many ways to improve the efficiency and the convergence speed. It is here to show the general if it is possible of the approach and if we can truly only calculate a subset of F^{-1} columns.

The objective function (4.5) minimizes the starlet components α . This objective leads again to a parabola in the one dimensional case, and we can analytically find the optimum for a single component when all others are fixed.

There are still a few problems to solve, like how to handle the matrix product $F^{-1}D$, With the active set heuristic, we iterate over a limited number of starlet components at a time.

The question remains, how the matrix product $F^{-1}D$ can be calculated efficiently. Since starlet transform is just made up of a couple of convolutions, we do not have to calculate the product $F^{-1}D$ explicitly. Convolutions in image space are multiplications in Fourier space. So for any starlet layer w_i or c_J , we can pre-calculate a transform vector. $w_2 = F^{-1}V * (\hat{S}_0\hat{S}_1 - \hat{S}_0\hat{S}_1\hat{S}_2)$

How many layers are needed. starlets rise in pixels with 2^J . Meaning if we want starlets over the whole image, the number of starlets rise logarithmically to the image dimensions.

How to iterate over the image in detail.

4.3 Iteration scheme

Many ways to iterate over the image. A simple scheme was used here.

Active set heuristic, find the starlets which are

```

1 def coordinate_descent(V_residual, x, lambda, max_iter):
2     for k in range(0, max_iter):
3         for i in pixels_row:
4             for j in pixels_column:
5                 x_old = x[i, j]
6                 fourier_column = calculate_fourier_transform(i, j)
7                 fr = real(fourier_column)
8                 fi = imag(fourier_column)
9                 rr = real(V_residual)

```

```
10      ri = imag(V_residual)
11
12      #find apex
13      a = sum(fr**2 + 2*fr*fi + fi**2)
14      b = sum(fr*rr + fr*ri + fi*rr + fi*ri)
15      x_new = b / a + x_old
16
17      x_new = shrink(x_new, lambda)
18      x[i, j] = x_new
19      V_residual = V_residual - fourier_column * (x_new - x_old)
```

coordinate descent with active set heuristic

sub-zero pixels

4.3.1 Non-uniform FFT approximations

Non uniform FFT to calculate the convolution KERNELS!!

Stupid approach with line search. Could be done more efficiently by using the histogram of the starlet level.

5 Test on Simulated Data

In this section, we test our new approach with Coordinate Descent on simulated MeerKAT data. We show that our approach does not need to calculate the whole Fourier Transform matrix F . Instead, we use a heuristic to only use relevant columns. As mentioned in section 4, it is unknown if our approach will converge to the true optimum. Nevertheless, we compare our results with CASA's CLEAN implementation, and demonstrate super-resolution performance of Coordinate descent together with accurate total flux modelling.

The two simulated datasets contains idealized MeerKAT observations. Compared to the real world, the two simulated datasets contain few Visibilities and not representative of the real data volume. Also, more realistic simulations which contain pointing-, calibration-, and thermal noise are out of scope for this project. The simulations are used to isolate the two fundamental issues in radio interferometer image reconstruction: Non-uniform sampling and incomplete measurements.

5.1 Super-resolution of two point sources

The first simulated observation contains two non-zero pixels, i.e. point sources, with intensity of 2.5 and 1.4 Jansky/Beam. The image has a size of 256^2 at a resolution of 0.5 arc-seconds per pixel. The integral, the total Flux of the image, is 3.9 Jansky/beam.

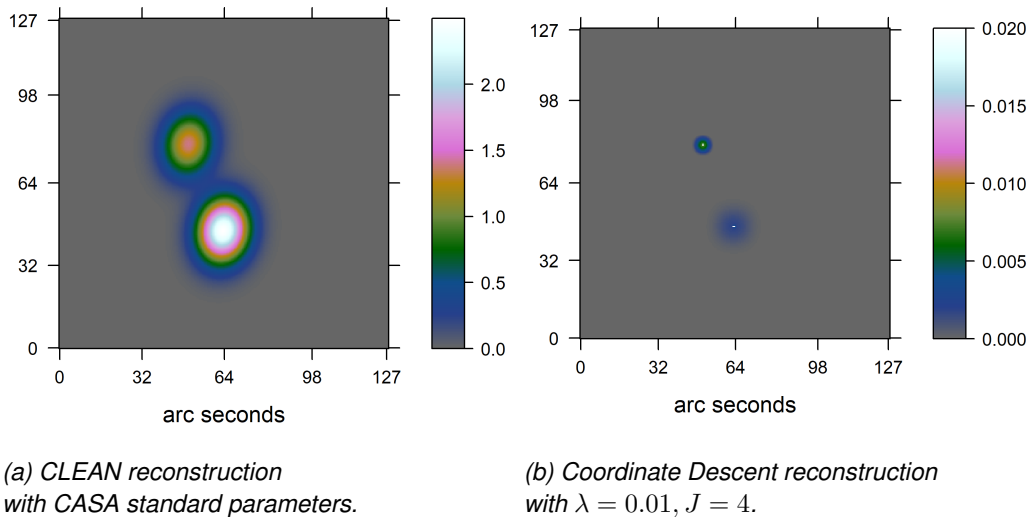


Figure 5: Image reconstruction of two simulated point sources.

The figure 5 shows the CLEAN and the Coordinate Descent reconstruction. CLEAN reconstructs the image 5a at the accuracy limit of the instrument. It essentially reconstructs a blurred version of the observed image, where the blurring represents the accuracy of the instrument. With compressed sensing, we aim to reconstruct the de-blurred image, increasing the effective accuracy of the instrument.

Coordinate Descent in image 5b shows a super-resolved reconstruction of the two point sources. It reconstructs two narrow peaks surrounded by a low-intensity Gaussian emission. Also, the total Flux of image 5b results in 3.92 Jansky/beam. The total flux of the CLEAN reconstruction 5a overshoots the 3.9 figure by a factor of 1400. This gets obvious when we compare the intensity profile of CLEAN, Coordinate Descent and the ground truth in figure 6.

Note that Coordinate Descent in figure 6 seems to have both point sources shifted by approximately a pixel.

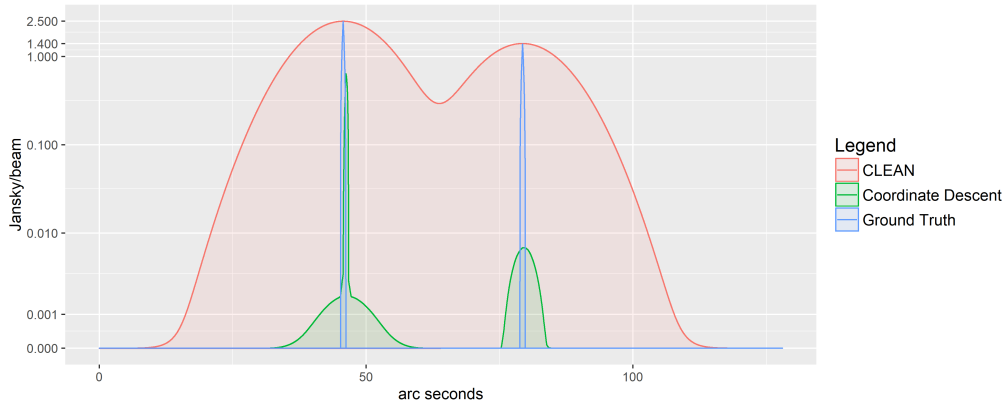


Figure 6: Intensity profile of the two point sources.

It looks suspiciously like an off-by one error. Sadly in the timeframe of this project, no error was found or an explanation for this behaviour.

, at a resolution of 0.5 arc-seconds per pixel.

The resolution of the image is therefore higher than MeerKAT. An ideal compressed sensing reconstruction would create an image where all pixels are zero except for the two point sources. Figure 5 shows the reconstructed images of CLEAN and Coordinate Descent.

The image 5b shows the Coordinate Descent reconstruction, which creates two much narrower peaks than CLEAN. This is an example of super resolution. Coordinate Descent located structures smaller than the accuracy of MeerKAT would allow.

The total Flux of the image, the sum of all emissions, is 3.9 Jansky/Beam in this simulation. CLEAN reconstructs the right peak intensities, both ending up at 2.5 and 1.4 respectively. Since CLEAN reconstructs a blurred version, the total Flux of the image is off by magnitudes. Figure 6 compares the intensity profile of CLEAN, Coordinate Descent and the Ground Truth. Note the logarithmic y scale. For a correct total flux, the integrals should be equal.

In the contour plot, the Coordinate Descents narrow contours become apparent.

The flux is sadly not correct, it seems to be too large by a factor of two

The larger source was well reconstructed. The second, smaller emissions however has a few issues.

note that the smaller emission is shifted by a pixel and the contour is wider than its larger cousin.

The last issue it has that the flux is still not correct. It is close and seems to be bigger than a factor of two.

Look at the flux in a more complex environment

5.2 Super resolution of mixed sources

Dataset of three gaussian extended emissions and sixteen point sources at varying intensities.

Parameters of Coordinate Descent

super resolution of CD. However, it did not find all point sources. Lets look closer at the flux reconstruction of extended emissions

Question of Flux reconstruction

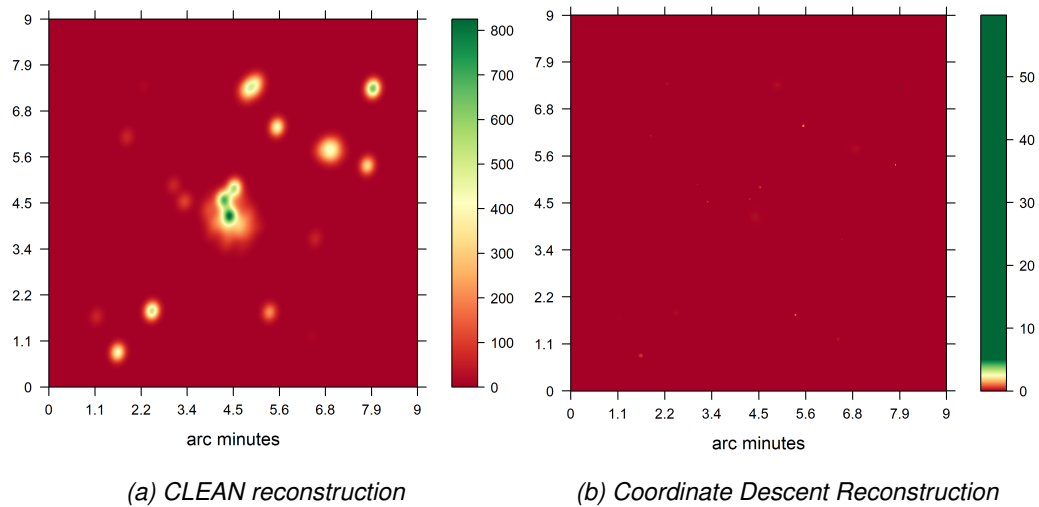


Figure 7: Reconstruction on mixed sources

λ for different starlet layers like in [5]

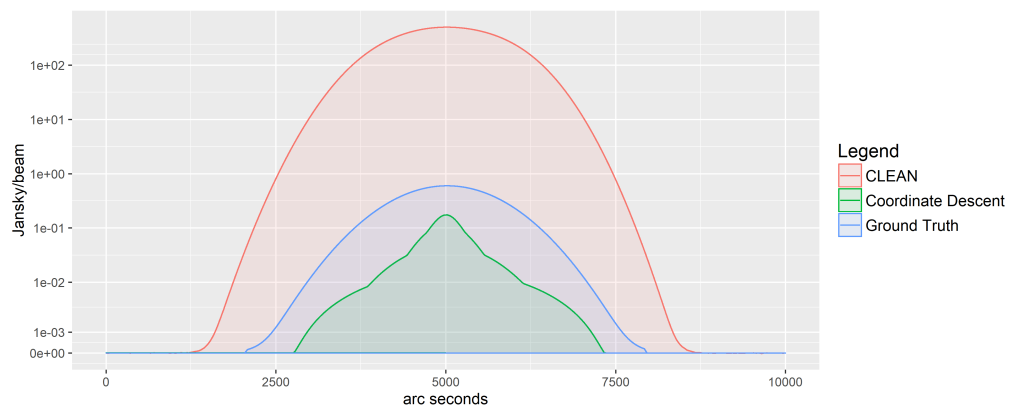


Figure 8: Reconstruction on mixed sources

Coordinate Descent did not reconstruct all point sources. How many starlets are non-zero is the major point for runtime. It depends on how many areas of the image are non-zero. Starlet has a representation for extended emission, how many starlets are needed for modelling is hard.

Runtime problems 1900 non-zero starlets,

6 Runtime cost comparison on a real-world MeerKAT reconstruction

Current Compressed Sensing reconstructions produce images at a higher quality than CLEAN. However, CLEAN is significantly cheaper to compute. MeerKAT's large scale reconstruction problems, CLEAN is still the go-to algorithm. In this project, we developed for a new architecture which hopefully reduces the cost of Compressed Sensing algorithms. The previous section 5 demonstrated super-resolution capabilities of our Coordinate Descent algorithm, which does not use the common Major Cycle architecture. The question, if our new approach can lower the runtime cost of Compressed Sensing reconstructions, is still open.

In this section, we compare the costs of our approach and WSCLEAN, which is the algorithm of choice for MeerKAT reconstructions. We create cost functions for each algorithm, counting the number of operations depending on the input size. WSCLEAN was executed on a real-world MeerKAT dataset, shown in image 9. Our proof-of-concept implementation was not able to handle the large dataset. Instead, we extrapolate the best-case costs of our approach and compare them to WSCLEAN on the MeerKAT dataset.

6.1 Cost function of an idealized Coordinate Descent

The runtime cost of Coordinate Descent depends on the number of Visibilities M and the number of non-zero starlets S . The number and location of the S non-zero starlets are generally not known. However, we created a heuristic which finds likely non-zero starlet components. In a realistic setting, the heuristic will have found more than S likely non-zero starlets. For the idealized version of Coordinate Descent, we assume an oracle performance heuristic: It finds the location and number of the S non-zero starlet components in constant time. Coordinate Descent therefore has to calculate the value of S components. In total, the idealized Coordinate Descent algorithm uses four steps: creating J starlet levels with the non-uniform FFT, creating the columns of F^{-1} , calculating the minima for each single component, and calculating the starlet layers:

$$\begin{aligned} & J \text{ non-uniform FFTs for the starlet regularization : } J * (M + 2N * ld(2N)) \\ & \quad \text{creating } S \text{ columns of } F^{-1} : S * 7M \\ & \quad \text{locating } S \text{ minima of } S \text{ parabolas : } S * 4M \\ & \quad \text{calculating } J \text{ Starlet layers : } J * 2M \end{aligned}$$

We assume we have enough memory to cache the columns of F^{-1} and only need to calculate them once. Keep in mind that each column of F^{-1} has the same length as the Visibilities, essentially multiplying the input data. The last parameter for Coordinate Descent is the number of iterations to converge, I_{CD} . Estimating this number is difficult as Coordinate Descent does not have strict guarantees (as discussed in section 4). Instead, we assume it converges after a fixed number of iterations. Therefore we arrive at the cost function of (6.1).

$$\begin{aligned} CD(I_{CD}, M, S, J) = & I_{CD} * [S * 4M + J * 2M] \\ & + S * 7M \\ & + J * (M + 2N * ld(2N)) \end{aligned} \tag{6.1}$$

Note that the runtime of Coordinate Descent is independent of the number of pixels. The only image related parameter in (6.1) is J , the number of starlet layers. The largest starlet layer represents the largest possible structure in the image, which is given by the instrument and the image resolution. The runtime only depends indirectly on the image resolution, not the total number of pixels. For simplicity, we assume the image cannot

have structures larger than half the image size. For our MeerKAT example, this is more than enough to represent the largest structures.

Also note the term iterating over the S non-zero starlets, $I_{CD} * [S * 4M + \dots]$. As it turns out, this is the Achilles heel of the algorithm. MeerKAT observations contain a very large amount of Visibilities M .

6.2 Cost function of WSCLEAN

The WSCLEAN algorithm uses the Major Cycle architecture. It uses the non-uniform FFT with w -stacking. The runtime costs of a single Major Cycle depends on the non-uniform FFT with w -stacking and the number of CLEAN deconvolutions. N denotes the number of pixels.

$$\begin{aligned} \text{non-uniform FFT : } & M + 2N * ld(2N) \\ \text{non-uniform FFT with } w\text{-stacking : } & M + W * (2N * ld(2N) + 2N) + N * ld(N) \\ I_{WSCLEAN} \text{ deconvolutions : } & I_{WSCLEAN} * 2N \end{aligned}$$

The overall cost function shown in (6.2) can also be split into two parts. In each Major Cycle, the forward and backwards non-uniform FFTs gets calculated, and CLEAN deconvolves the image for a certain number of iterations.

$$\begin{aligned} WSCLEAN(I_{Major}, I_{CLEAN}, M, N, W) = & I_{Major} * 2 * [M + W * (2N * ld(2N) + 2N) + NlogN] \\ & + I_{Major} * [I_{CLEAN} * 2N] \end{aligned} \tag{6.2}$$

Notice that the number of CLEAN deconvolutions I_{CLEAN} depends on the image content, similar the number of non-zero starlets S for Coordinate Descent. Here however, it multiplies with the number of pixels instead of the number of Visibilities. In a sense, the major cycle tries to reduce the runtime complexity of handling the image content by calculating the non-uniform FFT. If the difference is large enough $N \ll M$, then the Major Cycle will end up with a smaller runtime costs.

6.3 Comparison on a MeerKAT reconstruction problem

Our real-world MeerKAT observation has been calibrated and averaged in frequency and time to reduce storage space. The resulting dataset contains 540 channels with 4 million Visibilities each. Due to hardware limitations, WSCLEAN was calculated on 75 channels. The reconstructed image is shown in 9, and the resulting parameters for our cost function are:

- Major Cycles: $I_{Major} = 6$
- Number of CLEAN iterations: $I_{CLEAN} = 35'000$
- Visibilities: $M = 3.05e^8$
- Pixels: $N = 2048^2$
- w -stacks: $W = 32$

Set $J = 8$ For Coordinate Descent we need estimates for S and I_{CD} . We under-estimate the true values use them from our reconstruction of simulated MeerKAT data 7b. We it converges within $I_{CD} = 10$ iterations, our approach uses $10 * J$ iterations. Favourable assumption for Coordinate Descent. The reconstruction of the

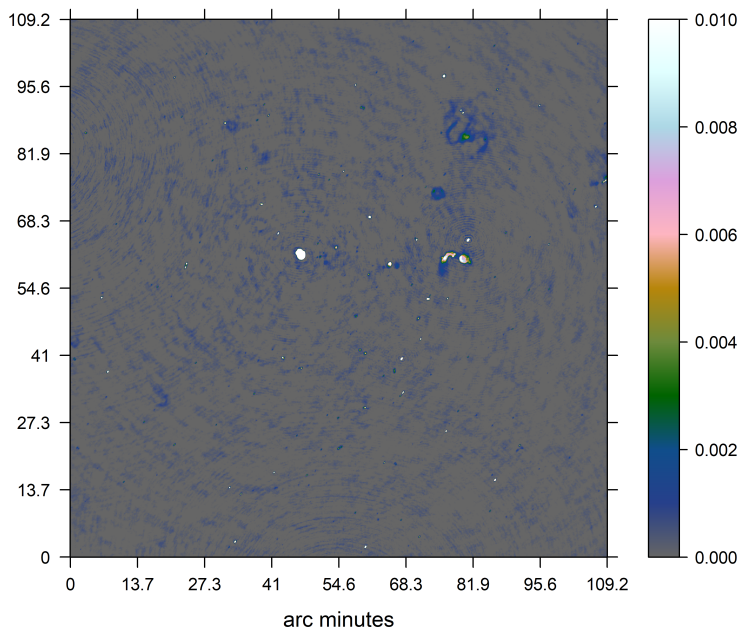


Figure 9: WSCLEAN Reconstruction of the MeerKAT observation.

MeerkAT image 9 has complex-shaped extended emissions. Approximating those with gaussian-like starlets likely leads to more non-zero starlets than 250.

When we put all values into our cost functions (6.1) and (6.2), CLEAN arrives at 1.9 times the costs of WSCLEAN. Mind you this is only when we can keep all necessary columns of F^{-1} in our memory, eating up 1.1 terabytes³ in our case. If not, the columns have to be re-calculated on the fly, increasing the runtime costs considerably.

Other compressed Sensing approaches. [9] reported 10 Major Cycles for a Compressed Sensing reconstruction on simulated data. If we plug in 10 Major Cycles in the WSCLEAN cost function for a rough estimate, we arrive at Coordinate Descent needing 1.2 the times of other compressed sensing approaches.

Coordinate Descent scales independently of image size. Pixel to Visibility ratio Note that the costs scale roughly linear to the pixels per Visibility ratio. The uncalibrated dataset contains 8 times more Visibilities. Due hardware limitations

The issue with Coordinate Descent's runtime complexity lies in the term $I_{CD} * [S * 4M + \dots]$ of (6.1), which scales with the "content" of the image S , multiplied with the Visibilities. Coordinate Descent cannot afford many iterations nor many non-zero components, because both of these numbers get multiplied together with M , the largest number in the problem. With the Major Cycle, WSCLEAN is able to get around this limitation, and scales any content dependant factors on N instead of M .

Indeed, the runtime of our Coordinate Descent algorithm could be improved by using the major cycle architecture, essentially replacing M with N and we arrive at the term $I_{CD} * [S * 4N + \dots]$. By using the Major Cycle architecture, Coordinate Descent can afford more iterations and more non-zero components in the image for the same runtime complexity. Furthermore N lies on a uniformly sampled grid. We may be able to use the FFT instead of caching columns of F^{-1} , and reduce the memory requirement at the same time.

³If we assume 64 bit floating point accuracy for the real and complex values of the Visibilities.

6.4 Embracing the Major Cycle

In this project, we created a Compressed Sensing reconstruction which works outside the Major Cycle architecture. With Coordinate Descent as optimization algorithm and starlets as regularization, it does not need the non-uniform FFT during reconstruction. Instead, it uses the relevant columns of the Fourier Transform matrix. We exploited the starlet regularization for estimating which columns are likely necessary for the reconstruction. This approach naturally extends to the wide field of view measurement equation (2.1). It can handle the w -term explicitly and does not need any w -term approximation algorithm. To our knowledge, this approach has not been explored previously for radio interferometer image reconstruction.

Proof-of-concept-implementation, as it is it may not converge to the true minimum. On Simulated dataset, it has Coordinate Descent created super-resolved point sources on simulated MeerKAT data. Compared to CLEAN, our reconstruction recovered the total flux accurately.

The question is if this approach has the potential to be cheaper than CLEAN. Can compressed sensing reconstructions reduce the runtime costs by getting rid of the Major Cycle. We extrapolated the minimum theoretical costs of our approach to a real-world MeerKAT observation and compared them with WSCLEAN. Sadly, our minimum estimate is approximately twice as expensive as WSCLEAN. With this approach, we did not improve upon the runtime costs of Compressed Sensing on large scale reconstructions.

Coordinate Descent costs scale the ratio between Visibilities and pixels. It is more cost effective, the more pixels we have per visibility. Intuitively, the major cycle reduces the costs, if we have a lot fewer Pixels than Visibilities. In our case, we have approximately 32 more Visibilities than pixels. Our approach scales independently of the image size, but the image size is a far smaller number in the MeerKAT reconstruction problem, which makes the Major Cycle architecture a sensible way to reduce costs. Indeed, our approach can potentially be reduced in costs by using the major cycle, even brush over the large memory requirement.

As it is, our approach does not lead to a runtime cost reduction. However, our approach is too accurate, we calculate the fourier transform in the area of mere floating-point inaccuracies. Not necessary, the instrument is more inaccurate than that. The Major Cycle exploits this with the non-uniform FFT approximation. Currently, we do it precisely.

Furthermore, we may not need all the Visibilities. Redundant information, can reconstruct the image with a subset of Visibilities. Hopefully self-calibration does not kill this idea.

With both, maybe there is a way to use this approach. It might be end up easier to distribute, because we do not need

Approach with other priors possible.

That does not mean our approach is useless. If we have a reconstruction problem, where

Scales with the ratio between Visibilities and

Question if this is the way to scale to large scale reconstruction. Our way is potentially easier to distribute, because it has plain matrix multiplications instead of approximation algorithms.

used an idealized algorithm to estimate the minimum runtime complexity. Turns out it is not competitive to other Major Cycle reconstructions. Each column of the Fourier Matrix has the length of the Visibilities. Massive Memory requirement on top of it. Sparsity depends on the prior. We could use different priors for reconstruction which may be more sparse, reducing the runtime and need for caching columns. However, the major cycle is just too competitive, we would need a VERY sparse prior in order to have a chance against Major Cycle reconstructions.

Indeed, even our Coordinate Descent algorithm can potentially be sped up with the Major Cycle, potentially getting rid of the massive memory requirement.

7 Compressed Sensing reconstructions in the MeerKAT era

MeerkAT poses a large scale reconstruction problem. Compressed Sensing approaches exist, they use the major cycle, but they all are slower to compute than CLEAN, for which the major cycle was developed.

It uses the non-uniform FFT to approximate the Fourier transformation of non-uniformly sampled Visibilities.

This project set out to explore different architectures for Compressed Sensing Reconstructions. A different way of getting from Visibilities to image.

Three different possibilities, with calculating the non-uniform FFT once, using spherical harmonics, or calculating only columns of the Fourier transform matrix

For the former, we created a novel approach which does not need the major cycle. We need a transformation, where we can both estimate which components are likely to be non-zero, and which use few non-zero components to represent an image.

This project used starlets, which were developed for astronomical images. Their solution is not sparse enough to scale to MeerKAT problems.

This leaves two other ways, splitting the major cycle falls off if we consider self-calibration

Spherical harmonics are the last way, Compressed Sensing algorithms have used it to gain another improvement in reconstruction quality. At this point, there is no Compressed Sensing algorithm which used the sphere for speed up.

here I see a possibility. The downside is it leads to a new measurement equation. It did not have as much time to formalize corrupting effects like antenna beam pattern, ionosphere and so on.

There is yet an

Still an open question

References

- [1] Emmanuel J Candès, Justin Romberg, and Terence Tao. Robust uncertainty principles: Exact signal reconstruction from highly incomplete frequency information. *IEEE Transactions on information theory*, 52(2):489–509, 2006.
- [2] David L Donoho. Compressed sensing. *IEEE Transactions on information theory*, 52(4):1289–1306, 2006.
- [3] JW Rich, WJG De Blok, TJ Cornwell, Elias Brinks, Fabian Walter, Ioannis Bagetakos, and RC Kennicutt Jr. Multi-scale clean: A comparison of its performance against classical clean on galaxies using things. *The Astronomical Journal*, 136(6):2897, 2008.
- [4] Urvashi Rau and Tim J Cornwell. A multi-scale multi-frequency deconvolution algorithm for synthesis imaging in radio interferometry. *Astronomy & Astrophysics*, 532:A71, 2011.
- [5] Julien N Girard, Hugh Garsden, Jean Luc Starck, Stéphane Corbel, Arnaud Woiselle, Cyril Tasse, John P McKean, and Jérôme Bobin. Sparse representations and convex optimization as tools for lofar radio interferometric imaging. *Journal of Instrumentation*, 10(08):C08013, 2015.
- [6] Arwa Dabbech, Alexandru Onose, Abdullah Abdulaziz, Richard A Perley, Oleg M Smirnov, and Yves Wiaux. Cygnus a super-resolved via convex optimization from vla data. *Monthly Notices of the Royal Astronomical Society*, 476(3):2853–2866, 2018.
- [7] Jasleen Birdi, Audrey Repetti, and Yves Wiaux. Sparse interferometric stokes imaging under polarization constraint (polarized sara). *arXiv preprint arXiv:1801.02417*, 2018.
- [8] Tim J Cornwell, Kumar Golap, and Sanjay Bhatnagar. The noncoplanar baselines effect in radio interferometry: The w-projection algorithm. *IEEE Journal of Selected Topics in Signal Processing*, 2(5):647–657, 2008.
- [9] Luke Pratley, Melanie Johnston-Hollitt, and Jason D McEwen. A fast and exact w -stacking and w -projection hybrid algorithm for wide-field interferometric imaging. *arXiv preprint arXiv:1807.09239*, 2018.
- [10] Luke Pratley, Jason D McEwen, Mayeul d’Avezac, Rafael E Carrillo, Alexandru Onose, and Yves Wiaux. Robust sparse image reconstruction of radio interferometric observations with purify. *Monthly Notices of the Royal Astronomical Society*, 473(1):1038–1058, 2017.
- [11] Jason D McEwen and Yves Wiaux. Compressed sensing for wide-field radio interferometric imaging. *Monthly Notices of the Royal Astronomical Society*, 413(2):1318–1332, 2011.
- [12] TD Carozzi. Imaging on a sphere with interferometers: the spherical wave harmonic transform. *Monthly Notices of the Royal Astronomical Society: Letters*, 451(1):L6–L10, 2015.
- [13] JD McEwen and AMM Scaife. Simulating full-sky interferometric observations. *Monthly Notices of the Royal Astronomical Society*, 389(3):1163–1178, 2008.
- [14] Nathanaël Schaeffer. Efficient spherical harmonic transforms aimed at pseudospectral numerical simulations. *Geochemistry, Geophysics, Geosystems*, 14(3):751–758, 2013.
- [15] J Richard Shaw, Kris Sigurdson, Ue-Li Pen, Albert Stebbins, and Michael Sitwell. All-sky interferometry with spherical harmonic transit telescopes. *The Astrophysical Journal*, 781(2):57, 2014.
- [16] Jason D McEwen, Gilles Puy, Jean-Philippe Thiran, Pierre Vanderghenst, Dimitri Van De Ville, and Yves Wiaux. Sparse image reconstruction on the sphere: implications of a new sampling theorem. *IEEE Transactions on image processing*, 22(6):2275–2285, 2013.

- [17] Stephen J Hardy. Direct deconvolution of radio synthesis images using l1 minimisation. *Astronomy & Astrophysics*, 557:A134, 2013.
- [18] Jean-Luc Starck, Fionn Murtagh, and Mario Bertero. Starlet transform in astronomical data processing. *Handbook of Mathematical Methods in Imaging*, pages 2053–2098, 2015.
- [19] Zhi-Quan Luo and Paul Tseng. On the convergence of the coordinate descent method for convex differentiable minimization. *Journal of Optimization Theory and Applications*, 72(1):7–35, 1992.
- [20] Jerome Friedman, Trevor Hastie, and Rob Tibshirani. Regularization paths for generalized linear models via coordinate descent. *Journal of statistical software*, 33(1):1, 2010.

List of Figures

1	The Major Cycle Framework	2
2	Celestial sphere distortion on simulated data. Source: [8]	5
3	Scaling and wavelet function of the starlet wavelet. Source: [18]	11
4	Dirty map and w_0 starlet layer. The right image shows the probability distribution for point sources in the dirty image.	12
5	Image reconstruction of two simulated point sources.	15
6	Intensity profile of the two point sources.	16
7	Reconstruction on mixed sources	17
8	Reconstruction on mixed sources	17
9	WSCLEAN Reconstruction of the MeerKAT observation.	20

List of Tables

8 Ehrlichkeitserklärung

Hiermit erkläre ich, dass ich die vorliegende schriftliche Arbeit selbstständig und nur unter Zuhilfenahme der in den Verzeichnissen oder in den Anmerkungen genannten Quellen angefertigt habe. Ich versichere zudem, diese Arbeit nicht bereits anderweitig als Leistungsnachweis verwendet zu haben. Eine Überprüfung der Arbeit auf Plagiate unter Einsatz entsprechender Software darf vorgenommen werden.

Windisch, January 23, 2019

Jonas Schwammburger